Magnesium-Mediated Electrochemical Synthesis of Ammonia

Ishita Goyal[a], Vamsi V Gande[a], Rajan R. Bhawnani[a], Rebecca Hamlyn[b], Ahmed A. Farghaly[c,d], and Meenesh R. Singh[a]*

[a] Department of Chemical Engineering, University of Illinois Chicago, Chicago, Illinois, 60607 United States

[b]Chemical Sciences Division, Lawrence Berkeley National Laboratory, Berkeley, California 94720, United States

[c]Chemical Sciences and Engineering Division, Argonne National Laboratory, Lemont, Illinois, 60439 United States

[d]Pritzker School of Molecular Engineering, The University of Chicago, Chicago, Illinois, 60637 United States

***Corresponding Author:**

Prof. Meenesh R. Singh
Associate Professor
Department of Chemical Engineering
929 W. Taylor St
University of Illinois Chicago
Chicago, IL 60607
Tel: (312) 413-7673
Email: mrsingh@uic.edu

Keywords: Electrochemical N_2 Reduction, Electrochemical NH_3 Synthesis, Li Mediated NH_3 Synthesis, Ca Mediated NH_3 Synthesis, Mg Mediated NH_3 Synthesis

Abstract

Metal-mediated electrochemical synthesis of ammonia (NH_3) is a promising approach to activate N_2 at room temperature. For instance, a lithium-mediated approach has been optimized to produce ammonia at high current density and selectivity. However, the scarcity of lithium and more negative plating potential pose limitations to scalability and energy efficiency. Alternative mediators have been proposed to address this challenge, but only calcium has shown some success, with NH_3 Faradaic efficiency (FE) of ~50%, while voltage requirements far exceed 3 V. Here we report a Mg-mediated nitrogen reduction reaction (Mg-NRR), where N_2 is activated on Mg to make nitride followed by its protolysis to make NH_3 coupled with regeneration of Mg sites. Notably, we achieved an NH_3 FE of 25.28 ± 3.80% at a current density of -45 mA/cm^2, which amounts to NH_3 current density of -11.30 ± 1.77 mA/cm^2 under 6 bar conditions. Isotope labelled experiments were performed to confirm the source of ammonia and yielded similar performance with an FE of 25.15 ± 1.01%. NH_3 production at the lowest total cell potential of 3V was demonstrated for the conversion of N_2 to NH_3. These promising results will motivate further research into these mediators and hold promise for enhancing the efficiency of electrochemical NH_3 synthesis.

Metal-mediated ammonia synthesis has garnered significant global attention as the only method capable of activating N_2 at ambient conditions and converting it into ammonia[1-7]. Among the various metal-mediated approaches, lithium-mediated nitrogen reduction reaction (Li-NRR) has been extensively studied and thoroughly explored[8]. Remarkable progress has been made, with Faradaic Efficiencies (FEs) for NH_3 production reaching nearly 100%, achieved through the use of imide-based lithium salts. Additionally, current densities as high as ~-700 mA/cm² have been reported. Fu et al.[9] advanced this method further by developing a continuous flow process, achieving a 61% NH_3 FE via hydrogen oxidation on a Pt-Au alloy anode.

Despite these advancements, Li-NRR still suffers from poor energy efficiency, notably lower than that of the traditional Haber-Bosch process[3], primarily due to the highly reducing electroplating potential of Li (~-3.04 V vs SHE)[3]. Moreover, the long-term stability of Li-NRR at high current densities is compromised by electrolyte degradation, which impairs lithium recovery and the high cost of lithium salts makes the process economically unfeasible. Selecting a metal with a lower reducing electroplating potential could significantly enhance energy efficiency. These limitations underscore the need to explore alternative metal-mediated systems that can offer improved stability and cost-effectiveness.

To explore these alternative mediators, the first challenge is to understand what makes lithium metal effective for ammonia production in a mediated process. The process proceeds with a series of electrochemical steps and chemical steps. The hypothesized mechanism involves Li deposition (electrochemical step) N_2 activation on lithium to form lithium nitride (chemical step), followed by its protolysis (chemical step) using a proton donor (e.g., ethanol) to generate NH_3, along with the regeneration of lithium sites. Based on the unique features of lithium including its stable nitride decomposition and optimal solid electrolyte interphase, which contribute to its exceptional selectivity, several criteria for a successful mediator of NH_3 electrosynthesis have been previously identified[10-18], including: (1) spontaneous nitride formation in the presence of N_2 (thermodynamics) and facile N_2 activation (kinetics), (2) stability of surface nitrogen vacancies in the nitride, (3) exergonic binding of N_2 at these surface vacancies, (4) solubility of mediator salts in non-aqueous electrolytes, and (5) facile diffusion of nitrogen in the bulk nitride.

In our previous work[19], we identified calcium and magnesium as potential mediators that meet these criteria, alongside lithium. These metals meet all the aforementioned criteria, with their surface nitride vacancies being more stable than bulk nitride vacancies and exhibiting spontaneous nitride formation at room temperature. Calcium (~-2.87 V vs SHE) has already been investigated in previous work, where it demonstrated favorable and stable performance, particularly using calcium perchlorate tetrahydrate and dimethoxy ethane as electrolyte. This system yielded a Faradaic efficiency (FE) of 50% for NH_3 production. Moreover, Fu et al.'s[20] work demonstrated the use of calcium as a mediator for nitrogen reduction in an electrochemical system, achieving a Faradaic efficiency of 40 ± 2%. This was the first study to rigorously verify calcium's ability to mediate ammonia synthesis in a continuous system, providing a critical step

toward utilizing earth-abundant elements for decentralized ammonia production under ambient conditions. Preliminary experiments with magnesium were also performed to show its ability as a successful mediator which achieved a FE of 27%[19]. A recent study by Krebz et al.[21] also reported NH_3 production in a Mg-mediated system with an FE of 7% where magnesium nitride was synthesized electrochemically and then immersed in an acidic solution to produce ammonia. They utilized a Cu foil electrode and an electrolyte composed of a mixture of Li and Mg salts, running their experiments at 33°C and 14 bar N2 pressure. The choice of electrolyte and electrode plays a significant role in ammonia synthesis, as it directly impacts the stability of the solid electrolyte interface (SEI). We, on the other hand, specifically selected ethanol (EtOH) as a weak proton donor, which helps reduce the protonation of magnesium, minimizing side reactions and enhancing overall system stability. Our approach, however, involves a more integrated process, synthesizing magnesium nitride and protonating it to form ammonia within the same cell, while simultaneously regenerating the magnesium sites. This simultaneous operation offers potential advantages in simplicity and efficiency for future optimization.

Building on this, we shifted our focus to magnesium, driven by its even lower plating potential (-2.37 V vs. SHE), making it a more efficient option. We hypothesize that Mg-mediated NH_3 synthesis occurs in a process analogous to Li and Ca mediated NH_3 synthesis, i.e., based on the reaction scheme 1. As illustrated in the scheme 1, upon the application of a negative current, Mg^{2+} ions begin to deposit on the cathode as metallic Mg (Mg^o). This Mg^o subsequently reacts with the available nitrogen, forming magnesium nitride (Mg_3N_2) on the cathode surface. The SEI formed during this process plays a crucial role in determining the functionality of the cell. If the SEI is sufficiently porous, it facilitates the transport of nitrogen to react with the Mg^o layer. The formed magnesium nitride undergoes protonation, releasing ammonia. This process creates nitrogen vacancies within the SEI, allowing another N_2 molecule to react with Mg^o, thereby sustaining the reaction cycle.

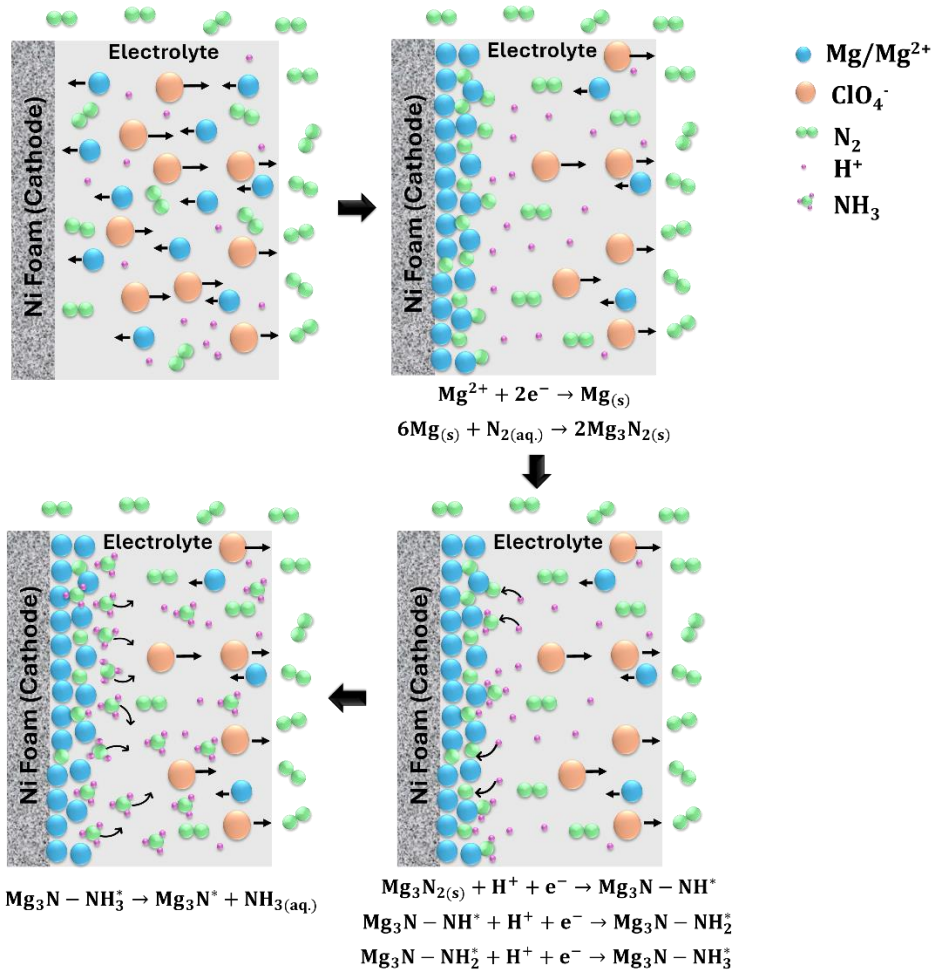

Scheme 1: Reaction schematic for Magnesium mediated ammonia synthesis

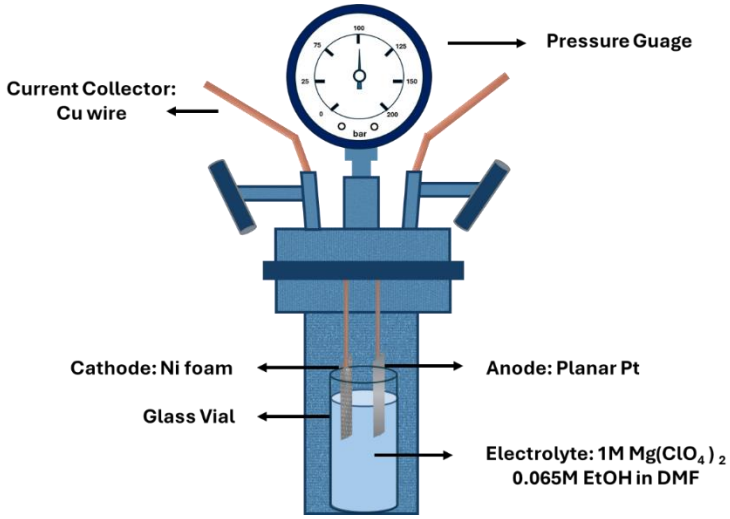

Figure 1: Schematic and configuration of the batch autoclave for electrochemical Mg mediated ammonia synthesis

In our previous investigation on Calcium and Lithium mediated ammonia synthesis[3, 19], we have identified an optimal concentration of the proton donor and N_2 pressure crucial for achieving a balance between Li_3N protolysis and Li protolysis steps. In line with these findings, for Mg-mediated NH_3 synthesis, we chose to operate the reactor at a N_2 pressure of 6 bars. Ethanol was designated as the proton donor, with a concentration of 0.065 M. To accommodate the high pressures required for the process, we implemented a modified autoclave setup. The schematic of experimental setup is shown in Figure 1 and actual image is shown in Figure S1. Within our experimental framework, Ni foam was employed as the cathode, complemented by Pt serving as the anode in a membrane less configuration. Maintaining a stirring rate of ~700 rpm ensured effective mixing of the electrolyte throughout the reaction. However, we encountered challenges with the solubility of magnesium salts in various solvents which were tested for Li-NRR and Ca-NRR, which proved to be quite limited and difficult to establish.

In metal nitride-mediated ammonia synthesis, the SEI plays a pivotal role in determining system performance. The selection of salt, solvent, and alcohol profoundly influences the composition and stability of the SEI, thereby affecting the FE of ammonia production. In lithium-mediated systems, salts such as $LiBF_4$[22], $LiClO_4$, and imide-based salts have been effectively utilized, underscoring the critical impact of salt selection on SEI characteristics and its subsequent effect on system stability and ammonia selectivity. The choice of magnesium salt was influenced by three key factors: solubility, conductivity, and SEI stability. Magnesium perchlorate was selected due to its high solubility in organic solvents like propylene carbonate and DMF, as well as its availability in anhydrous form. Its intermediate-sized perchlorate anion provided a balance between ionic conductivity and SEI stability, addressing the trade-off between these two properties. This combination ensured effective electrochemical performance with minimal iR losses and sufficient SEI stability for ammonia synthesis. The propylene carbonate system exhibited higher viscosity, leading to increased resistance and, consequently, reduced efficiency. A brief experimental protocol for the propylene carbonate system is provided in the SI. The system was tested at current densities of -2 mA/cm² and -30 mA/cm², but NMR analysis of the post-electrolysis samples showed no ammonia formation. Additionally, the voltage requirements for this system were extremely high, making it unsustainable for further investigation. The voltage and current data are included in Figure S7 of the SI.

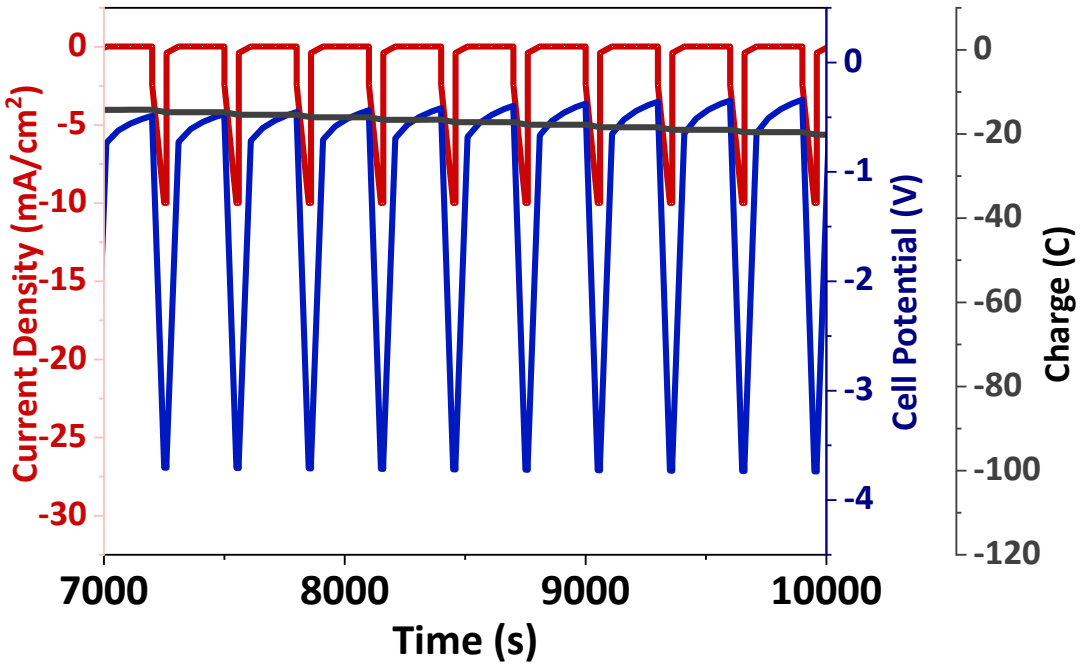

Figure 2: Chronopotentiometry analysis of Mg mediated ammonia synthesis at a current density of -10 mA/cm² (working phase – 1 min) and 0 mA/cm² (resting phase – 4 mins) and working potential range of 3.75-4 V. (Operating conditions: Electrolyte – 0.5M $Mg(ClO4)_2$ + 0.065M EtOH in dimethylformamide; 6 bar N2 pressure, Ni foam cathode and Pt anode).

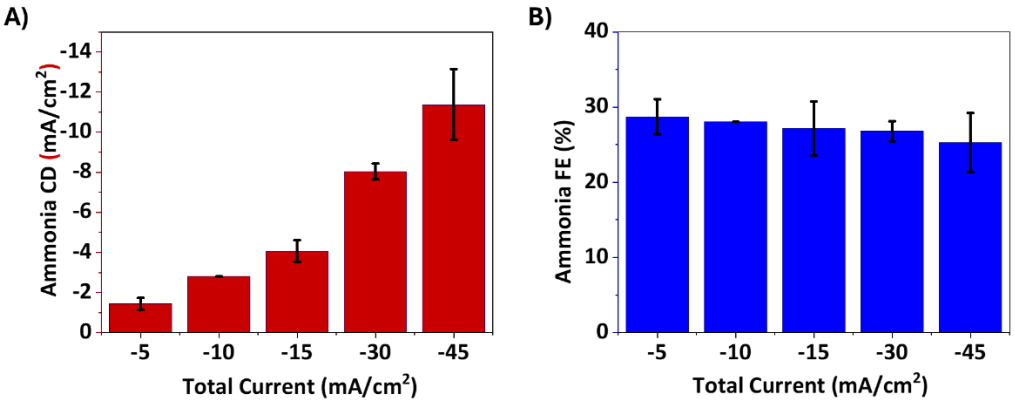

Figure 3: NH_3 current densities at different applied current densities B) and NH_3 FE at different applied current densities

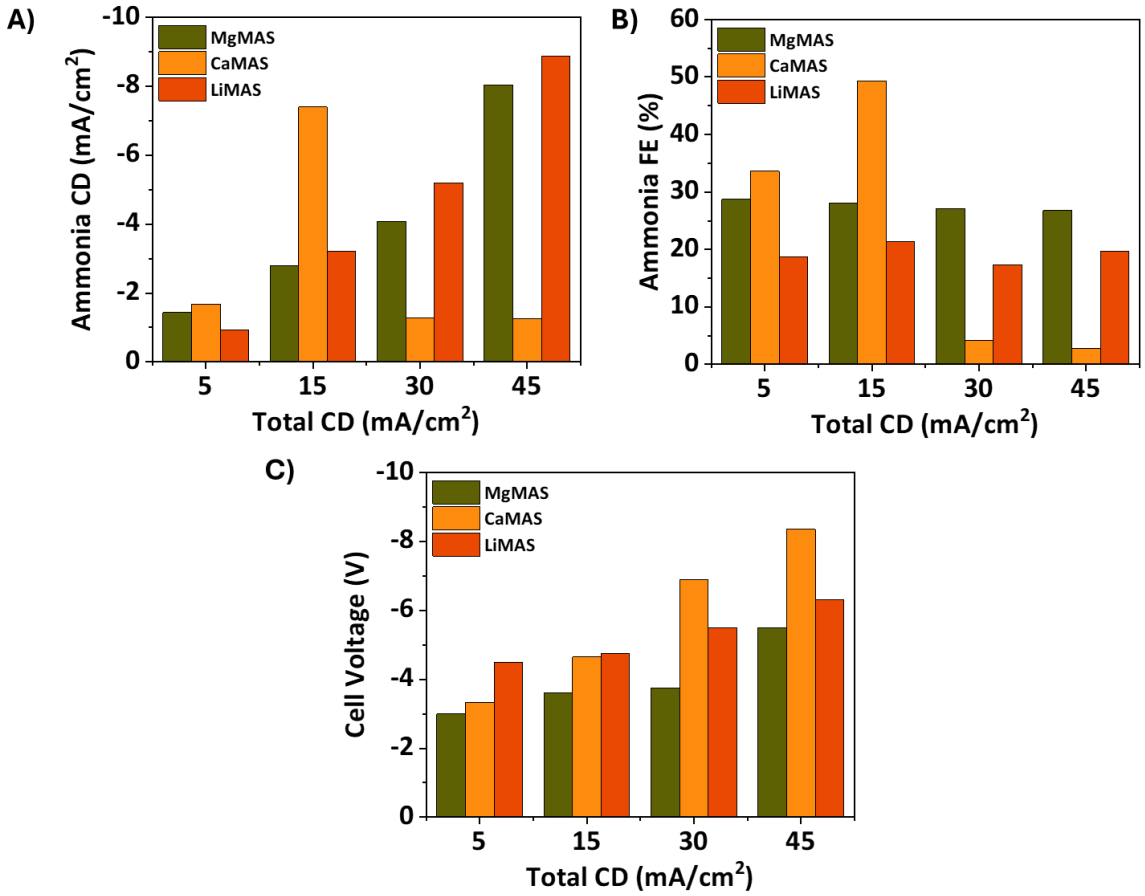

Figure 4: Comparison of NH_3 FE, NH_3 current densities and cell voltage for Li-NRR, Mg-NRR and Ca-NRR[3, 23]

The electrolyte comprised of 0.5M Magnesium perchlorate dissolved in DMF along with 0.065M EtOH. We implemented a current switching strategy following Andersen et al.'s recommendation[24], with 1 minutes of working time and 1-6 minutes of resting time (depending in the applied CD) to stabilize the SEI. The duration of the resting time varied and was adjusted as needed to maintain system stability, resulting in variable total runtimes for each current density. The resting current density was maintained at 0 mA/cm^2 (i.e., at open circuit voltage), while different working current densities were applied. Representative Chronopotentiometry for one applied current density of -10 mA/cm^2 is shown in Figure 2. Although this shows a zoomed in version to give a clear idea and visual representation of how current and potential values vary, the full graph is given in Si in Figure S6. The switching time is crucial for stabilizing cell voltage by limiting the growth of the SEI and preserving its stability. During the working time, when negative current density is applied, Mg deposition primarily occurs. The rate-limiting steps

during this phase include Mg nitridation, Mg_3N_2 protolysis, and Mg protolysis[3]. Conversely, during the resting time, when the current density is zero, Mg deposition ceases, and thermochemical nitridation and protolysis steps become dominant. The extent of Mg nitridation is contingent upon the N_2 pressure, while Mg_3N_2 protolysis and Mg protolysis are influenced by the concentration of the proton donor, ethanol. In our prior work on Li mediated ammonia synthesis[3] we observed that there are two distinct regimes: a proton-limited regime and an N_2 mass transfer-limited regime. When operating at lower nitrogen pressures, N_2 availability is relatively low, whereas protons are abundant in the solution. According to the hypothesized mechanism, under these conditions, N_2 mass transfer controls the rate of ammonia production. Conversely, at higher pressures, where N_2 is abundant for nitridation but the same amount of proton donor is used, protonation becomes the limiting factor for ammonia production. The reaction appears to proceed through two interconnected cycles: the nitridation loop and the protonation loop. Optimizing the frequency of these loops is critical for achieving the highest ammonia selectivity.

We hypothesize that the formation of the passivating SEI requires time to develop, approximately one hour under the reported conditions, and selectively permits the passage of Mg^{+2} ions, N_2, H_2, NH_3, and $H+$[3]. In metal-mediated systems, the oxidation of DMF at the electrode likely leads to the formation of a complex SEI composed of various organic and inorganic decomposition products. This SEI layer is critical for protecting the electrode surface and ensuring long-term system performance by being selectively permeable to magnesium ions while minimizing further reduction reactions. The formation of the SEI may involve mechanisms such as oxidation of reactions of organic solvents, similar to those observed in related systems like tetrahydrofuran (THF)[25], which undergo analogous degradation processes. While the SEI is beneficial for stabilizing the system, dissolved byproducts from the reaction between Mg and the solvent can negatively impact overall performance and ammonia selectivity. We hypothesize that once a stable SEI is formed, it enhances voltage stability by effectively suppressing further reduction of DMF at the electrode, thereby maintaining system integrity over time. Switching times also impact mass transport. It has been experimentally observed that during resting time, the open circuit potential should be maintained close to ~-0.1V to -0.5V depending on the current density. This condition is crucial for maintaining a stable and porous SEI, which facilitates the efficient mass transport of N_2 to the fresh Mg layer, enabling its nitridation. Without a stable and permeable SEI, nitrogen would be unable to penetrate and react with the deposited Mg, compromising the overall reaction process. Deviations from ~-0.1V to -0.5V favor H_2 formation through Mg protolysis. Thus, optimizing the resting time is crucial. Stirring speed also affects Mg_3N_2 and Mg protolysis and may vary based on the size and type of stirrer employed[3]. If the open circuit potential deviates significantly -0.5V, adjustments can be made to restore it. Lowering the resting time, working time, and stirring speed can bring the potential back to -0.1 to -0.5V if it drops below this value. Conversely, increasing the resting time, reducing the working time, and enhancing the stirring speed can restore the potential to -0.1 to -0.5V if it rises above this threshold. Based on our observations, we found that 1 minute of

working time and 1 up to 6 minutes of resting time are optimal for stabilizing the SEI depending on the total current density.

When the current density increases, the NH_3 current densities rise while the NH_3 FEs remain constant at an average value of ~27% as shown in Figure 3. The loss in FE could be attributed to excess Mg deposition, electrolyte breakdown, and corrosion. Figure 3 demonstrates that the production rates of NH_3 increase proportionally with rising current density. This suggests that the ratio of Mg protolysis to Mg_3N_2 protolysis rates is independent of potential, or perhaps both protolysis steps are barrierless at high potentials. Therefore, the potential-independent behavior could be due to a fixed fractional coverage of Mg_3N_2 on the cathode since protolysis is a thermochemical step. The coverage of Mg_3N_2 is balanced by nitridation and protolysis reactions, which are directly related to N_2 pressure and proton donor, respectively.

Figure 4 presents a comparison of FEs, ammonia current density and total cell voltage for Li-NRR, Ca-NRR, and Mg-NRR. For Mg and Li, we observed that an increase in total current density correlates with a proportional increase in ammonia production rate, while the FE for ammonia remains constant. This indicates that the NH_3 FE is independent of the applied current densities and the total cell potential for the configuration used. This also suggests that the same ammonia FE can be maintained even at higher current densities. Ca-NRR also shows significant potential with good ammonia selectivity, although further work is needed to enhance both the ammonia current density and FE. Mg-NRR, while promising, still requires in-depth research to achieve comparable FEs and current densities. When analyzing the applied potential trends for lithium, magnesium, and calcium in electrochemical systems, calcium exhibits higher potentials, primarily due to the lower salt concentration (around 0.5M calcium perchlorate) used in the system. Salt concentration plays a crucial role in electrochemical performance, as higher concentrations improve ion mobility, reduce solution resistance, and minimize ohmic losses. However, excessively high concentrations can increase solution viscosity, leading to higher resistance and degraded performance. For instance, in the LiNRR system, using $LIBF_4$ at concentrations of 1M to 3M significantly improved performance, but a 4M concentration caused performance degradation due to increased viscosity. Identifying the optimal salt concentration is therefore critical for achieving the best performance while managing costs, as higher salt concentrations can raise system expenses. Although a 1M calcium perchlorate solution resulted in lower Faradaic efficiency (FE), the 0.5M concentration was ultimately chosen as optimal due to its balance of performance and practicality. For lithium, a 2M concentration of lithium salt proved to be optimal, leading to a slightly lower applied potential compared to calcium systems. In the case of magnesium, a 1M concentration of magnesium perchlorate was initially employed in the previous study[19]. However, after 24 hours, the solution began to crystallize, prompting a reduction in concentration to 0.5 M. This adjustment prevented salt crystallization and ensured the solution remained well-mixed even 24 hours after the operation was completed. Comparable performance was achieved using 0.5 M magnesium perchlorate, which also demonstrated the lowest applied potential while maintaining satisfactory faradaic efficiencies (FEs). Among the three cations (Ca, Mg, and Li), magnesium emerges as the most promising mediator for ammonia synthesis. With a 0.5M concentration of magnesium perchlorate, it exhibits the low applied potential while maintaining high FEs. Mg shows significant potential for optimization due to its

favorable characteristics, such as a lower energy input compared to lithium and the ability to achieve relatively high FE under certain conditions. These traits suggest that, with further investigation and refinement of the reaction system, magnesium could become a promising candidate for efficient and sustainable ammonia synthesis. Furthermore, we observed that the working potential for Mg-NRR is relatively lower compared to Li-NRR and Ca-NRR, which aligns well with our hypothesis of a reduced plating potential for Mg. Notably, with Mg-NRR, we successfully synthesized ammonia at a working electrode potential as low as 3V.

Cyclic voltammetry (CV) was conducted in the same reaction set up to investigate the electrochemical behavior of magnesium in a 0.5M $Mg(ClO_4)_2$ electrolyte dissolved in DMF with 0.065M ethanol as a proton donor. The CV profile, recorded between -4 V and 4 V vs. Ag/AgCl at a scan rate of 10 mV/s, exhibits distinct cathodic and anodic features corresponding to magnesium deposition and stripping processes, respectively as shown in Figure S12. On the cathodic sweep, a significant current onset at approximately -2.45 V vs. Ag/AgCl indicates the reduction of Mg^{2+} ions to metallic magnesium on the working electrode. During the reverse anodic sweep, an oxidation peak is observed around 1.45 V vs. Ag/AgCl, signifying the stripping of deposited magnesium[26] back into the electrolyte as Mg^{2+}.

Open circuit control experiments were conducted where no potential was applied, and the solutions were stirred for 2 hours with 6 bars of N_2 pressure. NMR spectra of both pre-electrolyte and post-electrolyte samples showed no ammonia in the post-electrolyte samples, as shown in **Error! Reference source not found.**B. Additionally, another control experiment was performed using argon (Ar) to pressurize the reactor instead of N_2. The reactor was pressurized to 6 bar with Ar, and the reaction was carried out at -15 mA/cm^2 for 4 hours. Post-electrolyte analysis using ^{1}H NMR showed no ammonia peaks, as shown in Figure S5 in SI. Finally, an electrolyte sample was prepared and left open in the fume hood to ensure that ammonia was not originating from atmospheric contaminants but was instead being electrochemically synthesized. After 2 hours in the fume hood, ^{1}H NMR analysis showed no ammonia peaks as depicted in Figure S5 B in SI.

To evaluate the stability of the system in terms of operating potential and overall cell performance, long-term experiments were conducted over a total duration of 94 hours, including 47 hours of cumulative working time. The system operated under a cyclic chronopotentiometric mode, alternating between a working current density of -5 mA/cm² and a resting current density of 0 mA/cm², each for 1 minute. The cell exhibited smooth operation with stable potential values throughout, demonstrating the robustness and stability of the setup as shown in Figure S10. It should be noted, however, that this experiment was not designed to evaluate the stability of ammonia synthesis due to the membrane-less configuration of the cell. In such a setup, synthesized ammonia may be oxidized during extended periods of operation. The NMR quantification revealed the FE to be approximately 16%, which was half of what we observed during the 1-hour working time. This supports the claim that ammonia undergoes oxidation in the membrane-less setup.

Quantitative analysis of ammonia was conducted using ^{1}H NMR spectroscopy, following a previously published protocol that ensures the measured NH_3 arises from electrochemical N_2

reduction and not from air or other potential contamination sources[1]. The triplet peak associated with ammonia containing the most abundant $^{14}N_2$ isotope (spin 1 nucleus) appears at 6.83 ppm with a coupling constant of 96 Hz as shown in Figure 5A. The resulting spectra for the post-electrolyte samples at different current densities are depicted in Figure 5A. Isotope labelling and rigorous control experiments were performed to ensure that NH_3 is produced by the electrochemical reduction of N_2 and not from contaminants. Isotope labeling experiments were conducted at a current density of −45 mA/cm², as this condition resulted in the highest ammonia current density. The isotope-labeled samples were quantified using ^{1}H NMR, as shown in Figures 5C and 5D. These experiments yielded a Faradaic Efficiency (FE) of 25.15 ± 1.01%, with an ammonia current of 11.4 mA/cm² at −45 mA/cm². The NMR spectrum of ammonia generated from $^{15}N_2$ displays a characteristic doublet at 6.67 ppm, with a coupling constant of 96 Hz. UV-vis spectrometry was also used for quantification through the indophenol method. Both UV-vis and NMR were benchmarked and produced consistent results. The method of additions was employed to accurately determine the ammonia, as detailed in the SI.

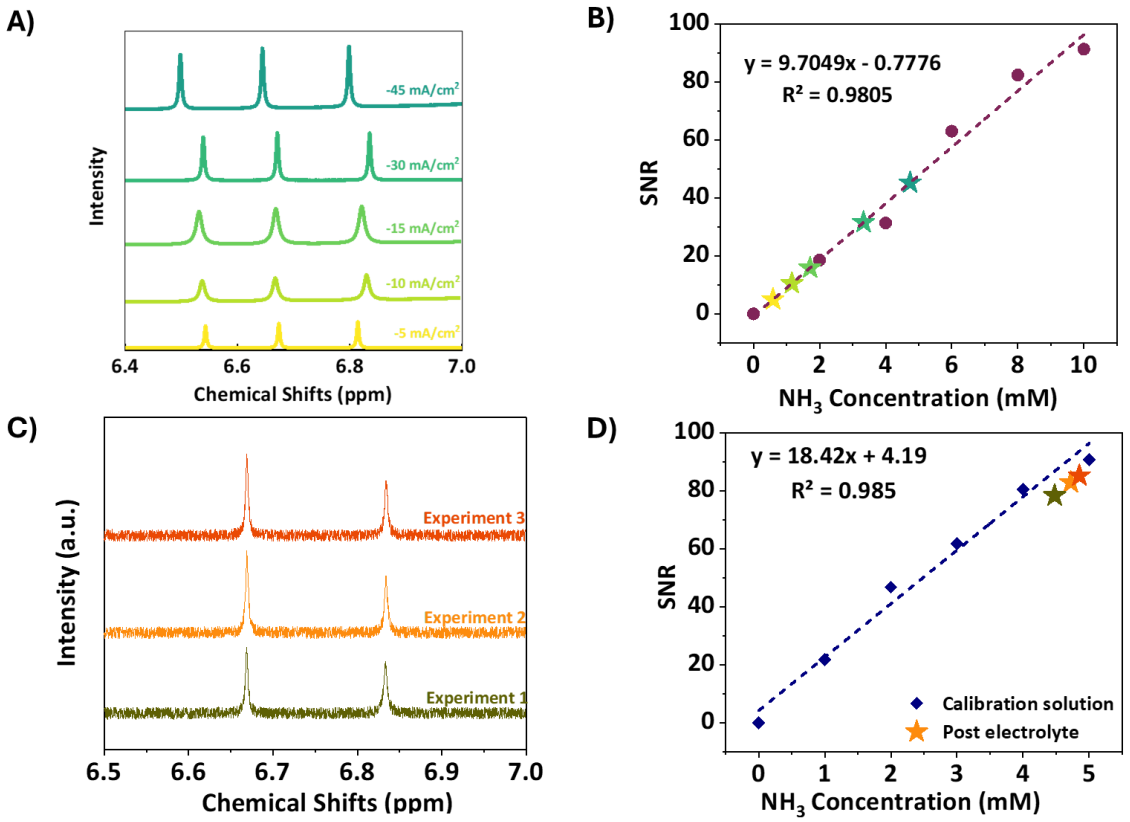

Figure 5: A) ^{1}H-NMR spectra of post-reaction electrolyte solutions collected at varying current densities. The current densities applied are labeled directly within the figure, and the spectra correspond to the ammonia detected in the electrolyte after the electrochemical reaction. B) Calibration curve generated from standard ammonia solutions (represented by dot symbols) prepared at known concentrations. The post-reaction product solutions (denoted by star symbols) are overlaid onto the calibration plot, with matching colors from Figure 5A to indicate

which spectra correspond to which current densities. C) ^{1}H-NMR spectra of Isotope labelled post-reaction electrolytes using $^{15}N_2$ performed at -45mA/cm^2 of current density D) Calibration curve generated from standard isotope labelled $^{15}NH_3$ ammonia solutions (represented by blue diamond symbols) prepared at known concentrations. The isotope labelled post-reaction product solutions (denoted by star symbol) are overlaid onto the calibration plot, with matching color from Figure 5C.

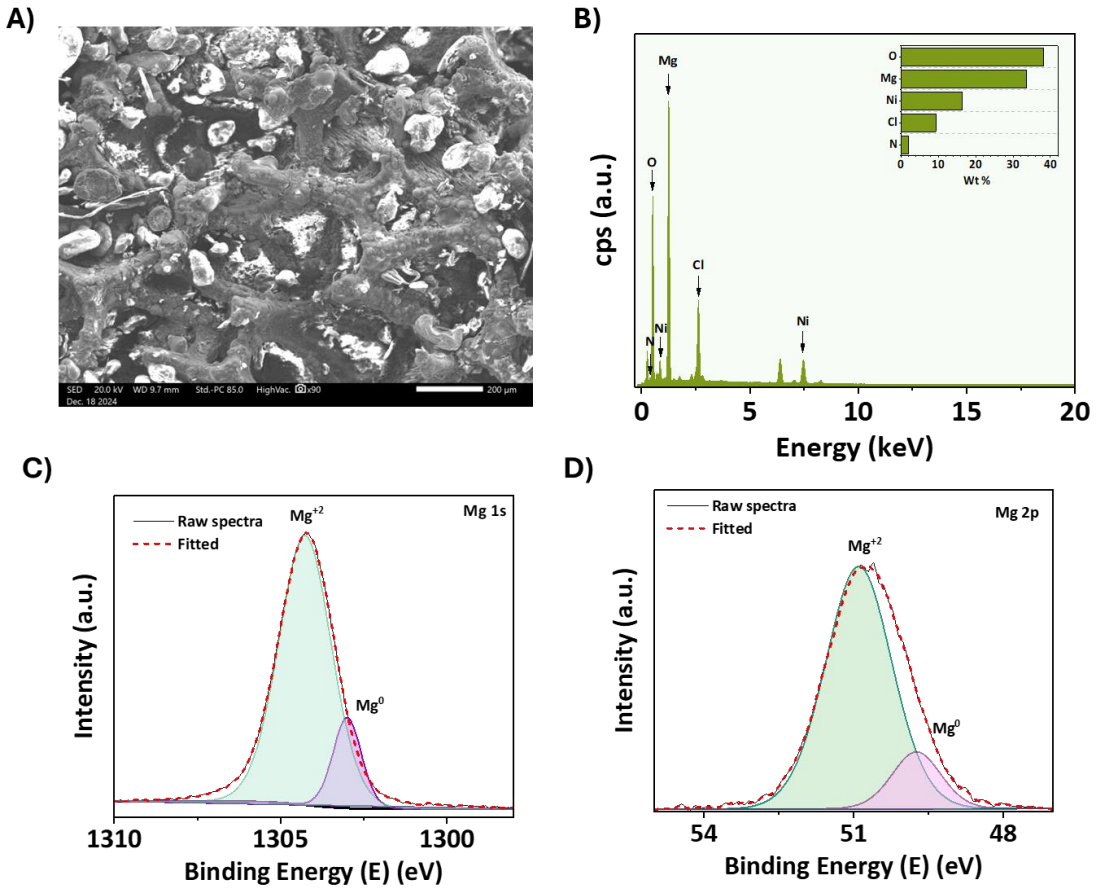

Figure 6: A) SEM image of Mg deposited Ni foam post electrolysis B) EDS spectrum of post electrolysis electrode showing the presence of Mg and Ni C) High resolution XPS scan of the post-electrolysis electrode confirming the presence of Mg^0 (1s) D) High resolution XPS scan of the post-electrolysis electrode confirming the presence of Mg^0 (2p).

The post-electrolysis catalyst was characterized using Scanning Electron Microscopy with Energy Dispersive X-ray Spectroscopy (SEM-EDS) and X-ray Photoelectron Spectroscopy (XPS) on the post-reaction sample, as illustrated in **Figure *1***Figure 6. In Figure 6C, a high-resolution XPS scan of the post-electrolysis electrode, confirming the presence of Mg^0 (1s) is shown, which strengthens the evidence of magnesium deposition during the electrochemical process. Similarly, Figure 6D shows a high-resolution XPS scan confirming the presence of Mg^0 (2p), providing further verification of magnesium deposition on the electrode surface. To resolve the uncertainty in XPS analysis about whether nitrogen signals originated from nitride formation or the nitrogen in DMF,

a 0.5 mm Ni foam sample was carefully prepared. This material was chosen because it could easily release any residual DMF at high temperatures and didn't retain a wet appearance. Magnesium was coated onto the Ni foam, and nitrogen gas (N_2) was bubbled continuously to encourage nitride formation. To protect the nitride layer from reacting with air, a thin layer of copper was deposited onto the Ni foam. The sample was then dried in a vacuum oven for 96 hours to ensure all traces of DMF were removed. Finally, a depth profile analysis was carried out to examine the SEI layers beneath the copper coating. Depth-profile XPS measurements were conducted to investigate the composition of the post-electrolysis catalyst using synchrotron-based XPS at the Advanced Light Source (ALS) at Lawrence Berkeley National Laboratory, specifically at beamlines 9.3.2 and 9.3.1. Tender X-rays with a photon energy of 4000 eV provided information from a depth of approximately 10–12 nm below the surface (Figure 7), while soft X-rays probed at a shallower depth of ~2–4 nm (Figure 7).

The successful electrodeposition of a relatively thick (>12 nm) Mg layer, along with the near-complete coverage of the nickel foam substrate, is evidenced by the absence of a nickel signal at the top surface of the catalyst (2-4 nm, probed at 900 eV) and a weak nickel signal in the XPS depth-profile at 10–12 nm (4000 eV).

Careful analysis of the Mg *1s* and *2p* core-level spectra, combined with the N *1s* spectrum, revealed that surface Mg species are primarily nitrogen-deficient, consisting of oxides, hydroxides, and carbonates[27, 28]. However, probing deeper into the catalyst layer (10–12 nm) with tender X-rays demonstrated the presence of nitrogen-rich Mg nitride phases. These are represented by broad peaks at ~1305 eV (Mg *1s*) and ~ 400 eV (N *1s*) , likely corresponding to Mg_3N_2 and possibly another nitride phase (e.g., MgN)[29]. The presence of nitride-related peaks suggests surface interactions between the deposited Mg and nitrogen during ammonia synthesis.

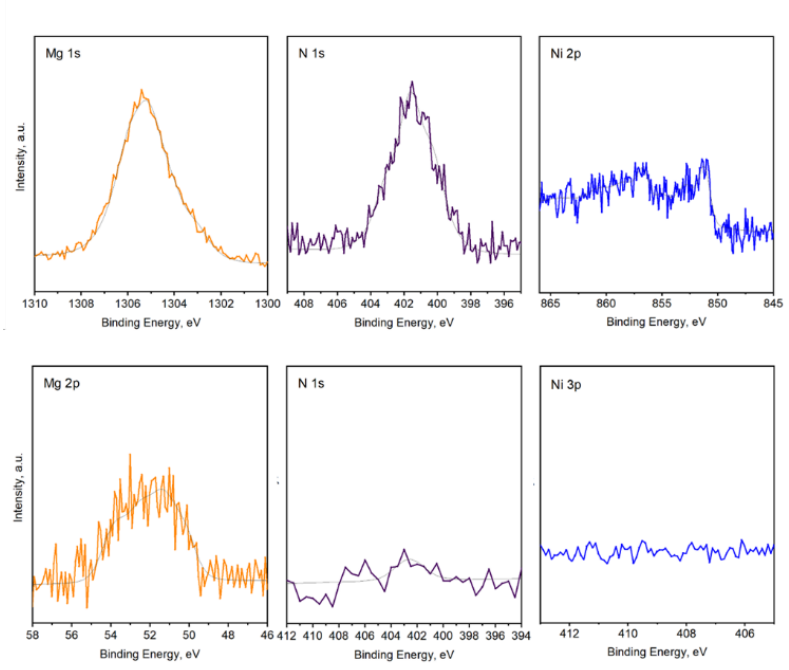

Figure 7: Depth-profiling XPS spectra for Mg *1s*, Mg *2p*, N *1s*, Ni *2p*, and Ni *3p* of the post-electrolysis catalyst. The top set was probed using tender X-rays at 4000 eV (10–12 nm), while the bottom set of spectra was recorded using soft X-rays at 900 eV (2–4 nm).

SEM-EDS analysis of the post-electrolysis Ni foam revealed the presence of Mg and N on the electrode, as demonstrated in the EDS mapping shown in Figure S11. To determine the physical characteristics of the SEI layer, we conducted the experiment using a polished planar metal electrode as the cathode. The cell setup remained the same, with the only difference being the replacement of the 3 mm Ni foam with the planar electrode. This facilitated faster drying of the solvent and provided clearer imaging of the SEI structure. SEM images and EDS mapping as shown in Figure S9 revealed the deposition of a thick SEI layer on the planar electrode. The mapping also showed a dense presence of Mg, further confirming that Mg deposition mediates the ammonia synthesis, supporting the direction of our hypothesized mechanism to a greater extent. These ex-situ analysis findings collectively reinforce the conclusion that Mg was successfully deposited during electrolysis. Although in situ analysis to understand the interface would be valuable, it is outside the scope of this work.

The research outlined in this letter provides an initial demonstration of Mg-mediated NH_3 synthesis, serving as proof of concept. We achieved a maximum NH_3 FE of 25.28 ± 3.8% at a current density of -45 mA/cm^2 which amounts to NH_3 current density of -11.3 ± 1.77 mA/cm^2. While lithium-mediated NH_3 synthesis (Li-NRR) has made significant progress, the scarcity of lithium and its highly negative plating potential (~-3.04 V vs SHE) limit scalability and energy efficiency. Calcium has been explored as an alternative, achieving NH_3 FE values around 50%, though with cell voltages exceeding 3 V, making it less practical. In contrast, this study presents a Mg-NRR process, where N_2 is activated on magnesium to form nitride, followed by its protolysis to produce NH_3, coupled with the regeneration of Mg sites. This approach demonstrates the potential for magnesium as a more sustainable and energy-efficient mediator, paving the way for future research into Mg and other metals beyond lithium for ammonia production. In this study, we validated our theoretical hypothesis of a reduced plating potential for Mg compared to Li and Ca. Remarkably, using Mg-NRR, we achieved ammonia synthesis at a working electrode potential as low as 3V. Furthermore, we found that NH_3 FE remains constant for various current densities. However, the process encounters several challenges that must be addressed for further development. One major obstacle is the limited solubility of Mg salts in the solvents explored in this study. Future investigations should focus on screening the solubility of different Mg salts in various aprotic solvents. This exploration would facilitate the testing of different salt and electrolyte configurations for Mg-mediated NH_3 synthesis, ultimately leading to an optimal setup to maximize NH_3 FE and lower the total cell potential, thereby enhancing the overall energy efficiency of the process. Additionally, the role of the SEI in determining NH_3 FE remains poorly understood. In-situ studies to probe the SEI are necessary to gain insights into its influence on the synthesis process. Overall, the findings presented here pave the way for future research on NH_3 synthesis utilizing Mg and other materials beyond lithium as potential mediators.

Acknowledgement:

This work made use of the EPIC facility of Northwestern University's NUANCE Center, which has received support from the SHyNE Resource (NSF ECCS-2025633), the IIN, and Northwestern's MRSEC program (NSF DMR-1720139). This work also made use of the Keck-II facility of Northwestern University's NUANCE Center, which has received support from the SHyNE Resource (NSF ECCS-2025633), the IIN, and Northwestern's MRSEC program (NSF DMR-2308691). This work made use of the IMSERC at Northwestern University, which has received support from the NSF (CHE-1048773 and DMR0521267).

This work was supported in part by the U.S. Department of Energy, Office of Science, under contract DE-AC02-06CH11357.

The Advanced Light Source is supported by the Director, Office of Science, Office of Basic Energy Sciences, of the U.S. Department of Energy under Contract No. DE-AC02-05CH11231.

References:

1. S. Z. Andersen, V. Čolić, S. Yang, J. A. Schwalbe, A. C. Nielander, J. M. McEnaney, K. Enemark-Rasmussen, J. G. Baker, A. R. Singh, B. A. Rohr, M. J. Statt, S. J. Blair, S. Mezzavilla, J. Kibsgaard, P. C. K. Vesborg, M. Cargnello, S. F. Bent, T. F. Jaramillo, I. E. L. Stephens, J. K. Nørskov and I. Chorkendorff, *Nature*, 2019, **570**, 504-508.
2. H.-L. Du, M. Chatti, R. Y. Hodgetts, P. V. Cherepanov, C. K. Nguyen, K. Matuszek, D. R. MacFarlane and A. N. Simonov, *Nature*, 2022, **609**, 722-727.
3. N. C. Kani, I. Goyal, J. A. Gauthier, W. Shields, M. Shields and M. R. Singh, *ACS Appl Mater Interfaces*, 2024, **16**, 16203-16212.
4. K. Kim, S. J. Lee, D. Y. Kim, C. Y. Yoo, J. W. Choi, J. N. Kim, Y. Woo, H. C. Yoon and J. I. Han, *ChemSusChem*, 2018, **11**, 120-124.
5. N. Lazouski, M. Chung, K. Williams, M. L. Gala and K. Manthiram, *Nature Catalysis*, 2020, **3**, 463-469.
6. J. A. Schwalbe, M. J. Statt, C. Chosy, A. R. Singh, B. A. Rohr, A. C. Nielander, S. Z. Andersen, J. M. McEnaney, J. G. Baker, T. F. Jaramillo, J. K. Norskov and M. Cargnello, *ChemElectroChem*, 2020, **7**, 1542-1549.
7. A. Tsuneto, A. Kudo and T. Sakata, *Journal of Electroanalytical Chemistry*, 1994, **367**, 183-188.
8. Y. H. Junwen CAO, Yun ZHENG, Wenqiang ZHANG, Bo YU, *Front. Energy*, 2024, **18**, 128-140.
9. X. Fu, J. B. Pedersen, Y. Zhou, M. Saccoccio, S. Li, R. Sažinas, K. Li, S. Z. Andersen, A. Xu, N. H. Deissler, J. B. V. Mygind, C. Wei, J. Kibsgaard, P. C. K. Vesborg, J. K. Nørskov and I. Chorkendorff, *Science*, 2023, **379**, 707-712.
10. A. R. Singh, Ph.D. Dissertation, Stanford University, 2019.

11. A. R. Singh, B. A. Rohr, M. J. Statt, J. A. Schwalbe, M. Cargnello and J. K. Nørskov, *ACS Catalysis*, 2019, **9**, 8316-8324.
12. Y. Abghoui, A. L. Garden, J. G. Howalt, T. Vegge and E. Skúlason, *ACS Catalysis*, 2016, **6**, 635-646.
13. Y. Abghoui, A. L. Garden, V. F. Hlynsson, S. Björgvinsdóttir, H. Ólafsdóttir and E. Skúlason, *Physical Chemistry Chemical Physics*, 2015, **17**, 4909-4918.
14. Y. Abghoui and E. Skúlason, *The Journal of Physical Chemistry C*, 2017, **121**, 6141-6151.
15. Y. Abghoui and E. Skúlason, *Catalysis Today*, 2017, **286**, 78-84.
16. N. D. Lang, S. Holloway and J. K. Nørskov, *Surface Science*, 1985, **150**, 24-38.
17. A. Lausche and J. Norskov, *318142 Effects of Coverage Dependent Adsorbate-Adsorbate Interactions for CO Methanation On Transition Metal Surfaces*, 2013.
18. R. Tort, A. Bagger, O. Westhead, Y. Kondo, A. Khobnya, A. Winiwarter, B. J. V. Davies, A. Walsh, Y. Katayama, Y. Yamada, M. P. Ryan, M.-M. Titirici and I. E. L. Stephens, *ACS Catalysis*, 2024, **14**, 3169-3170.
19. I. K. Goyal, Nishithan; Olusegun, Samuel; Chinnabattigalla, Sreenivasulu; Bhawnani, Rajan; Glusac, Ksenija; Singh, Aayush; Gauthier, Joseph; Singh, Meenesh, *ACS Energy letters*, 2024, DOI: acsenergylett.4c01455.
20. X. Fu, V. A. Niemann, Y. Zhou, S. Li, K. Zhang, J. B. Pedersen, M. Saccoccio, S. Z. Andersen, K. Enemark-Rasmussen, P. Benedek, A. Xu, N. H. Deissler, J. B. V. Mygind, A. C. Nielander, J. Kibsgaard, P. C. K. Vesborg, J. K. Nørskov, T. F. Jaramillo and I. Chorkendorff, *Nat Mater*, 2024, **23**, 101-107.
21. M. Krebsz, R. Y. Hodgetts, S. Johnston, C. K. Nguyen, Y. Hora, D. R. MacFarlane and A. N. Simonov, *Energy & Environmental Science*, 2024, **17**, 4481-4487.
22. X. Fu, S. Li, N. H. Deissler, J. B. V. Mygind, J. Kibsgaard and I. Chorkendorff, *ACS Energy Letters*, 2024, **9**, 3790-3795.
23. I. Goyal, N. C. Kani, S. A. Olusegun, S. Chinnabattigalla, R. R. Bhawnani, K. D. Glusac, A. R. Singh, J. A. Gauthier and M. R. Singh, *ACS Energy Letters*, 2024, DOI: 10.1021/acsenergylett.4c01455, 4188-4195.
24. S. Z. Andersen, M. J. Statt, V. J. Bukas, S. G. Shapel, J. B. Pedersen, K. Krempl, M. Saccoccio, D. Chakraborty, J. Kibsgaard, P. C. K. Vesborg, J. Nørskov and I. Chorkendorff, *Energy & Environmental Science*, 2020, **13**, 4291-4300.
25. R. Sažinas, S. Z. Andersen, K. Li, M. Saccoccio, K. Krempl, J. B. Pedersen, J. Kibsgaard, P. C. K. Vesborg, D. Chakraborty and I. Chorkendorff, *RSC Advances*, 2021, **11**, 31487-31498.
26. Z. Yang, M. Yang, N. T. Hahn, J. Connell, I. Bloom, C. Liao, B. J. Ingram and L. Trahey, *Frontiers in Chemistry*, 2022, **10**.
27. V. Fournier, P. Marcus and I. Olefjord, *Surface and Interface Analysis*, 2002, **34**, 494-497.
28. F. Khairallah and A. Glisenti, *Surface Science Spectra*, 2007, **13**, 58-71.
29. D. Höche, C. Blawert, M. Cavellier, D. Busardo and T. Gloriant, *Applied Surface Science*, 2011, **257**, 5626-5633.